PCCP

PAPER

View Article Online
View Journal | View Issue

Cite this: *Phys. Chem. Chem. Phys.*, 2014, **16**, 21688

Pressure induced manifold enhancement of Li-kinetics in FCC fullerene

Deya Das,[a] Sang Soo Han,[b] Kwang-Ryeol Lee[b] and Abhishek K. Singh*[a]

Received 22nd July 2014,
Accepted 19th August 2014

DOI: 10.1039/c4cp03251a

www.rsc.org/pccp

The reduction of the diffusion energy barrier for Li in electrodes is one of the required criteria to achieve better performances in Li ion batteries. Using density functional theory based calculations, we report a pressure induced manifold enhancement of Li-kinetics in bulk FCC fullerene. Scanning of the potential energy surface reveals a diffusion path with a low energy barrier of 0.62 eV, which reduces further under the application of hydrostatic pressure. The pressure induced reduction in the diffusion barrier continues till a uniform volume strain of 17.7% is reached. Further enhancement of strain increases the barrier due to the repulsion caused by C–C bond formation between two neighbouring fullerenes. The decrease in the barrier is attributed to the combined effect of charge transfer triggered by the enhanced interaction of Li with the fullerene as well as the change in profile of the local potential, which becomes more attractive for Li. The lowering of the barrier leads to an enhancement of two orders of magnitude in Li diffusivity at room temperature making pressurized bulk fullerene a promising artificial solid electrolyte interface (SEI) for a faster rechargeable battery.

1 Introduction

Li ion batteries are the most popular energy storage devices in the recent decades due to their smaller size and high energy density.[1–3] However, the energy density achieved so far is not sufficient to meet the demand of current generation portable electronic devices or hybrid cars.[4–7] Finding a better anode material, which has a high specific capacity compared to the commercially available graphite (372 mA h g^{-1}) anode is the biggest challenge.[8–10] While silicon has the highest theoretical capacity of 4200 mA h g^{-1},[11,12] the large volume expansion during charging/discharging creates cracks, resulting in the continuous formation of a solid electrolyte interface (SEI), which eventually breaks the electrical contacts. By reducing the size of the Si anode, making it in the form of nanoparticles and nanowires,[13–15] volume change and fracture can be prevented. It has also been proposed that carbon based materials such as graphene or fullerene when coated on silicon electrodes can act as an artificial SEI and restrict the volume expansion.[16,17] The success of this approach depends on achieving faster Li kinetics in such materials, which is essential for ensuring quicker charging–discharging rates.

In the case of pristine multilayer graphene, it has been shown experimentally as well as theoretically, that the Li diffusion barriers are very high, almost preventing any through diffusion[18–20] thereby rendering it ineffective as an artificial SEI. Bulk and polymerized phases of fullerene[21] are considered as another promising contender for an artificial SEI. Li diffusion barriers on a surface of a single fullerene between two binding sites namely the center of a hexagon and pentagon[22] are found to be reasonably low. The barrier can be further reduced in the FCC bulk fullerene[23] structure, where the presence of a large number of voids could help Li diffuse even faster. Polymerized fullerene, a close analogue to the bulk, has been shown[17,24–26] to work as an interesting coating material for the Si anodes. Polymerized fullerene coated on a Si anode using a plasma evaporation technique[17] has shown excellent electrochemical performance and it depends on the extent of polymerization.

In order to evaluate the electrochemical performance of bulk as well as polymerized fullerene as an artificial SEI, we study Li diffusion in bulk fullerene. Using first principles density functional theory based calculations we scanned the potential energy surface of bulk fullerene and obtained a minimum energy path for Li diffusion with a low barrier of 0.62 eV. It has been shown that the polymerization can be achieved by applying pressure to the bulk fullerene phases.[27,28] Hydrostatic pressure was applied to the bulk fullerene to study the polymerized fullerene structure. Surprisingly, the Li diffusion barrier decreases rapidly with the applied pressure up to a critical value corresponding to 17.7% volume strain beyond which the barrier starts to increase again. The applied pressure induces a rapid charge transfer from the Li to the fullerene structure, therefore, facilitating faster kinetics. Furthermore, the applied pressure alters the profile of electrostatic potential near the transition

[a] *Materials Research Centre, Indian Institute of Science, Bangalore 560012, India. E-mail: abhishek@mrc.iisc.ernet.in*
[b] *Korea Institute of Science and Technology, Hwarangno 14-gil 5, Seongbuk-gu, Seoul 136-791, Korea*

state by making it more attractive for Li thereby reducing the energy barrier further. This reduction in the diffusion barrier causes an enhancement of two orders of magnitude in the diffusivity of Li, making pressurized bulk fullerene an excellent candidate for artificial SEI.

2 Methodology

The calculations were performed using first principles based density functional theory (DFT) as implemented in the Vienna *ab initio* simulation package (VASP).[29,30] Electron–ion interactions were described using all-electron projector augmented wave (PAW) pseudopotentials.[31] Electronic exchange and correlation were expressed by the Perdew–Burke–Ernzerhof functional of the generalized gradient approximation.[32,33] In the bulk FCC fullerene structure, C_{60} clusters are bound by weak van der Waals forces. To incorporate this effect, Grimme's DFT-D2 method[34] has been used, where a semi-empirical dispersion potential has been added to the conventional Kohn–Sham DFT energy, through a pair-wise force field. The conventional FCC fullerene unit cell containing 240 atoms was used for all the calculations. Due to the large size of the unit cell the Brillouin zone was sampled by the Γ point. The conjugate gradient scheme was employed to relax the structures until the component of forces on each atom were ≤ 0.005 eV Å^{-1}. In order to ensure the accuracy of the calculations, the kinetic energy cutoff for the plane wave was set to 400 eV.

3 Results and discussion

We consider a conventional FCC unit cell for bulk fullerene having four C_{60} clusters, as shown in Fig. 1(a). The choice of conventional unit cell over the primitive cell allows individual C_{60} to rotate and relax. The bigger size of the unit cell helps to capture the details of the potential energy surface (PES) comprehensively. There are four octahedral and eight tetrahedral voids in a FCC unit cell. Due to the presence of these voids, Li is expected to diffuse faster. The optimized lattice parameter is found to be 14.31 Å, which is in good agreement with the experimental value[35,36] of 14.20 Å. The carbon atoms in neighbouring C_{60} clusters interact *via* van der Waals forces[23] and the minimum distances among them is $\sim$3.4 Å.

The potential energy surface has been scanned by a computationally inexpensive single point calculation with $10 \times 10 \times 10$ grid points. It gives an estimate to locate the low energy points and the path connecting these points gives the most probable diffusion path for Li. In Fig. 1(b), the positions of Li within 1 eV above the minimum energy structure have been shown. The minimum energy path for Li diffusion is shown in Fig. 1(a) where Li positions are marked by red solid spheres. This minimum energy path connects alternately tetrahedral and octahedral voids in the FCC structure. In a conventional unit cell of a FCC fullerene, there are two such paths. The energy barrier for Li diffusion is high in octahedral voids and energy minimas are obtained in tetrahedral voids (Fig. 1(c)). The Nudged Elastic Band (NEB) method[37] is used to get an accurate value of the energy barrier along the same path. The NEB results are qualitatively similar to the single point calculations. The maximum energy barrier of 0.62 eV is found at the centre of octahedral void. Though the barrier is slightly higher than the barrier in a conventional graphite anode of 0.4–0.48 eV,[38,39] Li can overcome this barrier easily under proper charging–discharging conditions.

In real systems, the Li diffusion barriers at the surface would be different. An estimate of this barrier can be obtained from

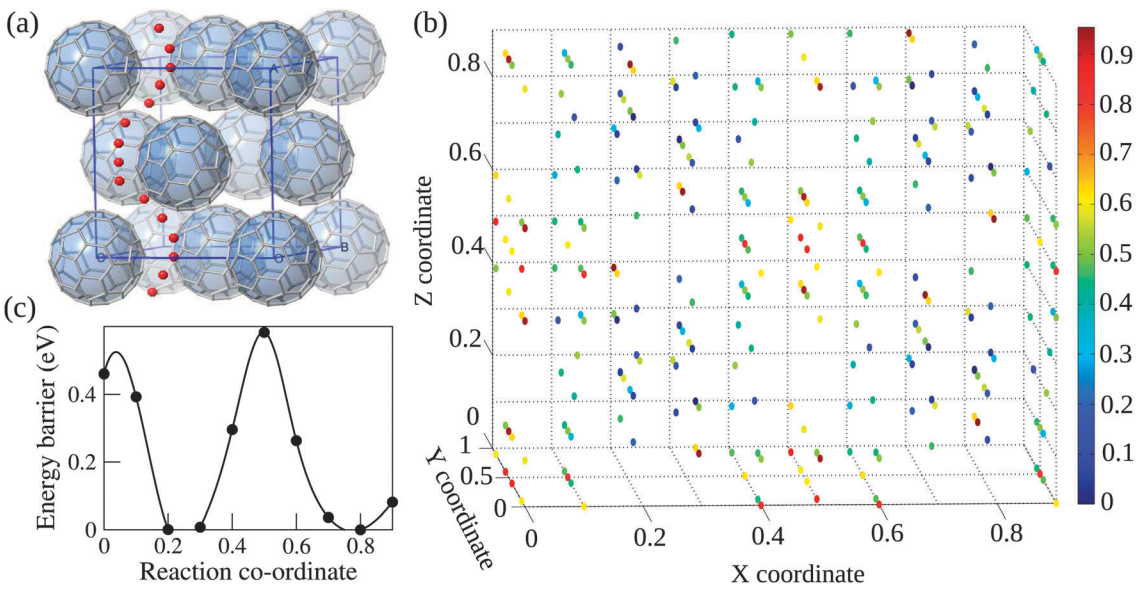

Fig. 1 (a) Li diffusion path where Li positions are marked by red solid spheres in the FCC fullerene structure, (b) potential energy surface of FCC fullerene up to 1 eV with respect to the minimum energy value. The points with barriers higher than 1 eV have been removed from the graph. The variation of energy barrier has been described by the color coded bar denoting maxima by red and minima by blue. All three axes denote three lattice vectors in fractional coordinates. (c) The corresponding energy barrier of Li along a minimum energy path obtained by single point calculations.

the calculations carried out for the single fullerene surface.[22] The barriers corresponding to the different diffusion paths are much lower (~0.11–0.15 eV) than the lowest barrier inside the bulk. Therefore, the surface barrier would not affect the diffusion of Li in an artificial SEI based on a few layers of bulk fullerene.

Experimentally it has been observed that polymerization in the fullerene leads to better electrochemical performances[17,24–26] and it is enhanced with a greater extent of polymerization.[17] There are various reports of polymerized fullerene achieved by applying hydrostatic pressure.[27,28,40] In order to model polymerized fullerene, hydrostatic pressure has been applied by decreasing the lattice parameter with respect to the optimized value of 14.3 Å. The volume strain (ε) associated with hydrostatic pressure is calculated as follows:

$$\varepsilon = \frac{V_0 - V}{V_0}$$

where V_0 and V denote the relaxed volume and instantaneous volume of the FCC fullerene structure, respectively. The different values of lattice parameters and corresponding strain and pressure are shown in Table 1. The corresponding pressure has been calculated using the formula:

$$P = \frac{E - E_0}{V_0 - V}$$

where E_0 and E denote the total energy value for the relaxed and pressurized fullerene FCC structure, respectively. The application of strain or pressure reported in our study is experimentally feasible.[40,41] The structures are fully relaxed at each applied strain value. The structure remains the same under the applied strain except the relative changes in the orientation of the fullerenes. The C–C bond lengths in fullerene decrease and the internal voids becomes smaller with the strain. Beyond 23.1% strain, inter-fullerene bond formation occurs with bond lengths in the range of 1.51–1.55 Å. Experimentally, it has been reported that at room temperature, the FCC fullerene structure retains its stability up to 20 GPa of applied hydrostatic pressure.[40] Another experimental study reported that under 5 GPa pressure and synthesis temperatures between 300° and 400 °C, a FCC fullerene structure with a lattice parameter of 13.6 Å[41] exists. Therefore, given the progress in the experimental synthesis of the pressurised fullerene structures, it would not be difficult to apply the pressure reported in our study.

Next, we calculate the Li energy barrier as a function of applied strain. The minimum energy path remains almost the same except at two points at which the Li deviates from the path slightly. The deviation is caused by the change in orientation of the fullerenes in the relaxed structure with the increasing applied hydrostatic pressure. The application of pressure lowers the energy barrier in octahedral voids. The values of energy barrier for different strain values are listed in Table 1. Fig. 2(a) shows that up to 17.7% strain, the energies of almost all of the intermediate images along the reaction path including the transition state (Li at the center of octahedral void) reduce. The minimum energy barrier is found to be 0.46 eV at 17.7% volume strain. Further enhancement of the pressure increases the energy barrier as shown in Fig. 2(b). The trend of the variation of energy barrier with applied volume strain is plotted in Fig. 2(c).

The effect of the reduction of the barrier on the Li diffusion is studied by calculating the diffusivity, *i.e.*, the proportionality constant between the flux due to diffusion and the gradient in the concentration. Diffusivity of Li at a particular temperature $D(T)$ can be obtained by knowing the energy barrier E_b from the Arrhenius equation

$$D(T) = D_0 e^{-E_b/k_B T}$$

where the pre-exponential factor D_0 is a constant and independent of temperature and k_B is the Boltzmann constant. At a volume strain of 17.7%, the diffusivity at room temperature (300 K)

Table 1 Lattice parameter (a), corresponding volume strain (ε), pressure (P) and energy barrier (E_b) are listed below

a (Å)	ε (%)	P (GPa)	E_b by NEB (eV)
14.3	0	0	0.62
14.0	6.2	0.27	0.55
13.7	12.1	0.33	0.51
13.4	17.7	1.19	0.46
13.1	23.1	2.44	0.48
12.8	28.3	3.53	0.52
12.5	33.2	5.59	0.76

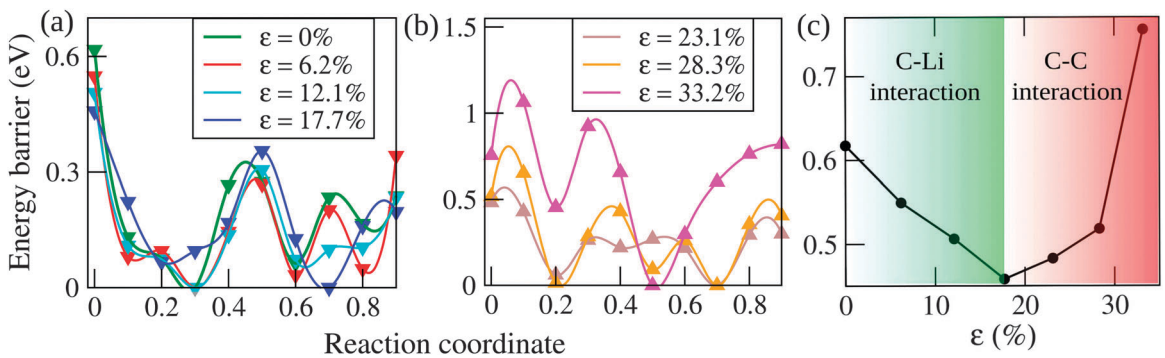

Fig. 2 Plots of Li diffusion energy barrier calculated using NEB along the diffusion path in the FCC fullerene structure with increasing pressure: (a) up to 17.7% strain, energy barrier decreases, (b) beyond 17.7% strain, energy barrier increases. (c) Maximum value of the energy barrier for Li at the octahedral void as a function of increasing strain.

increases by a factor of $e^{-(0.46-0.62)/k_BT} \sim 487.51$ compared to an unstrained case, thereby, enhancing the diffusion rate of Li by two orders of magnitude. This enhancement in diffusivity would lead to an unprecedented increase in the charging–discharging rate of the battery.

This manifold enhancement is very exciting but in several aspects it is counter intuitive. For example, why is there an energy barrier at the octahedral void whereas there is an energy minima at the tetrahedral site? The diffusion should also slow down with the applied pressure as it makes the voids smaller. Last but not least why would the barrier increase again after a volume strain of 17.7%? In order to answer these questions, we analysed the density of states (DOS) of the system without Li under applied strain as shown in Fig. 3(a). The band gap obtained in unstrained FCC fullerene is ~0.75 eV that matches well with the reported value.[36,42] With the increasing applied pressure, the band gap decreases and the distance between buckyballs reduces leading to covalent bond formation between C atoms of different buckyballs.[43,44] At the strain value of 17.7% the DOS becomes finite at the Fermi level closing the band gap. With the further increase in strain, the DOS becomes completely delocalized denoting stronger interaction between the carbon atoms of different fullerenes. This pressure induced band gap decrease and subsequent metallic transition enhance the conductivity of the FCC fullerene, which partially explains the improved electrochemical performances in polymerized fullerene.

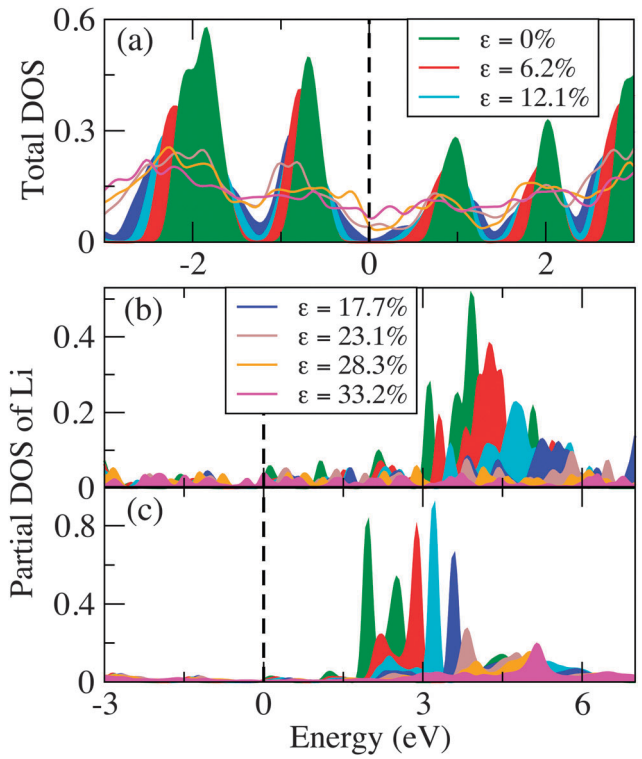

Fig. 3 (a) Total density of states (DOS) of the FCC fullerene structure without Li as a function of applied hydrostatic pressure. Up to 17.7% volume strain, the DOS has been plotted by solid color to show the change in band gap and beyond that, by a solid line to denote the delocalization in it. Partial DOS of Li-2s in the FCC fullerene structure with Li as a function of applied hydrostatic pressure (b) at the tetrahedral void and (c) at the octahedral void.

In the presence of Li in the FCC fullerene, DOS becomes finite even at zero pressure. With increasing pressure the DOS gets delocalized indicating the enhanced interaction of Li with the underlying bulk fullerene. To get a better insight, partial DOS (PDOS) of Li-2s is calculated and plotted in solid color in Fig. 3(b) and (c) corresponding to the Li position at the tetrahedral and octahedral voids, respectively. The peak in PDOS above the Fermi level denotes that Li is ionized. The shift in this peak from the Fermi level, gives a measure of the Li–C interaction. The PDOS shows that for the tetrahedral void, the Li-2s peak is at a higher energy compared to the octahedral void. This indicates that the interaction as well as charge transfer are more when Li is in the smaller tetrahedral void than the bigger octahedral void. Therefore, there is an energy barrier at the octahedral site and an energy minima at the tetrahedral site. This feature does not change with increasing strain. Moreover, as the applied strain increases, the peak shifts to the higher energy up to 17.7% strain demonstrating an enhancement in the interaction of Li with fullerene. This enhancement in the Li–C interaction with increasing applied volume strain causes the lowering of the barrier up to 17.7% volume strain. Beyond this critical strain, the peak position does not change much and the PDOS becomes completely delocalized and hence no further decrease in the barrier observed.

To understand the reason for the increase in the barrier height beyond the volume strain of 17.7%, the PDOS corresponding to the C-2s and C-2p orbitals for the carbon atoms that are closest in two adjacent fullerenes, have been plotted in Fig. 4 with blue and orange solid colors, respectively. At higher strain values of 28.3% and 33.2% the hybridization between the C-2s and C-2p states becomes very strong, indicating the covalent bond formation between two neighbouring fullerenes. Because of this bond formation the Li gets repelled and the barrier height goes up making it difficult for Li to diffuse. The analysis of DOS clearly explains that, due to the stronger interaction of Li with fullerenes, the diffusion energy barrier goes down with increasing strain value up to 17.7%. With the subsequent increase in strain, the interaction between carbon atoms of neighbouring fullerenes becomes dominant, which hinders the Li diffusion.

In order to understand why the increasing charge transfer lowers the diffusion barrier, we next study the changes in the local electrostatic potential, as a function of applied pressure. The planar averaged electrostatic potential of FCC fullerene plotted along the (100) direction, shown in Fig. 5, is symmetric around the center. At the centre of the octahedral void the potential profile shows a double peak. However, at the center of the tetrahedral void a dip is observed. In the presence of Li in the central octahedral void, the potential profile is modified. In Fig. 5, the upper (lower) dashed line denotes the peak value of the potential without (with) Li. With the increasing pressure the peak at the octahedral site decreases up to an applied strain of 17.7%. This lowering of the peak makes the profile of potential more attractive for the Li, therefore, improving the binding energy and eventually lowering the barrier. With the further increase in the strain, the peak at the octahedral site starts to increase, leading

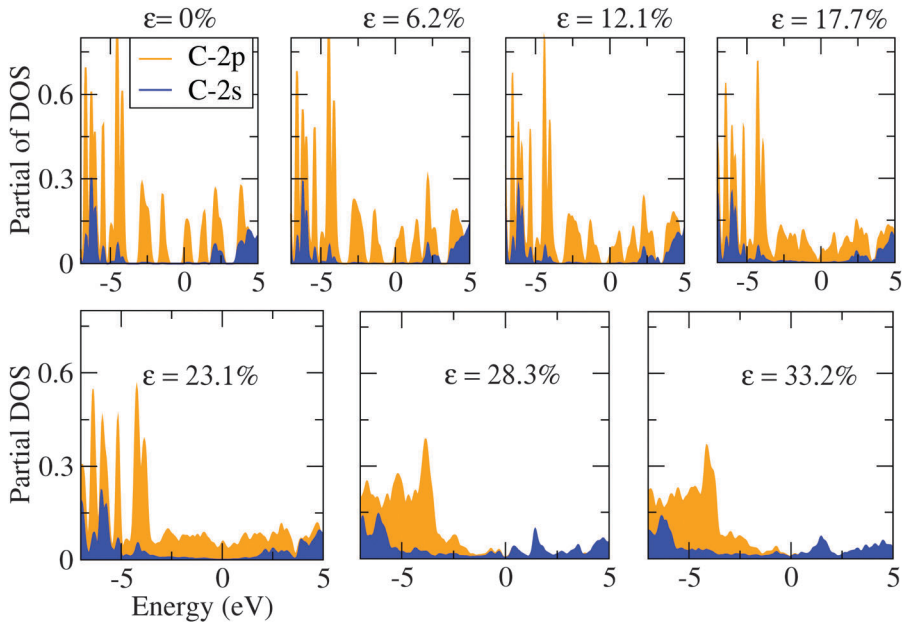

Fig. 4 PDOS of the C atom near the octahedral void that takes part in bond formation between two C_{60} balls under pressure. The value of PDOS for the C-2s orbital has been enhanced for better visualization.

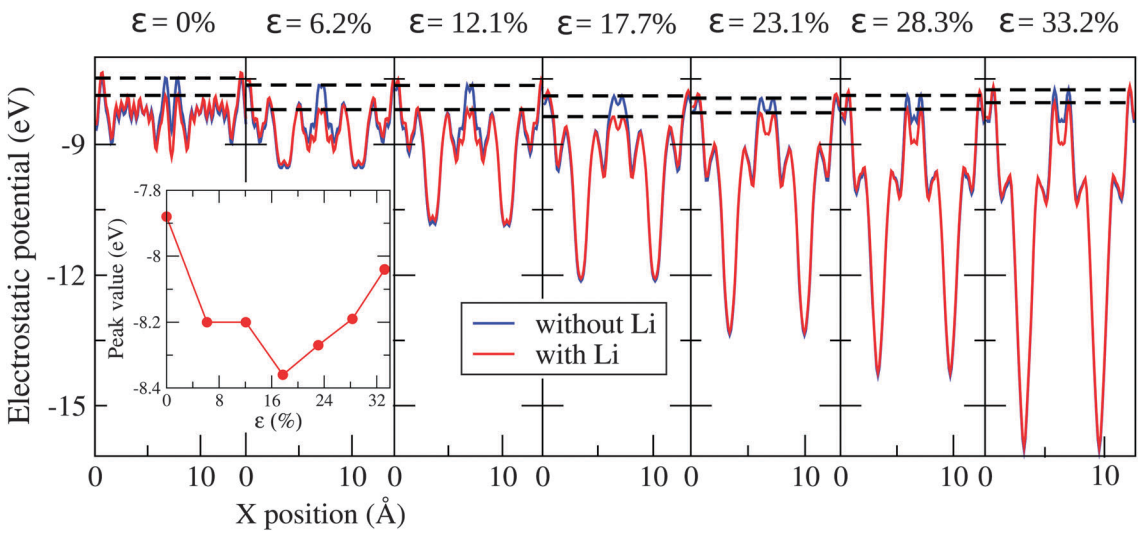

Fig. 5 Plane-averaged electrostatic potential with *x* position of the FCC fullerene under increasing volume strain. The dashed horizontal lines denote the peak position of potential without and with Li in the central octahedral void from the top. Inset: the peak position of plane-averaged electrostatic potential in the presence of Li is plotted with volume strain.

to enhancement of the barrier. The peak value of the total local potential profile in the presence of Li with increasing strain is plotted in Fig. 5 inset. The trend observed here matches very well with the change in the diffusion barrier with the applied strain. Therefore, the modification of the profile of the local potential plays an important role in controlling the diffusivity of Li.

4 Conclusion

In summary, we have studied the possibility of using the bulk phase of fullerene as an artificial solid electrolyte interface in a Li ion battery. The Li diffusion path was determined by scanning the potential energy surface. The most probable path includes Li diffusion through the tetrahedral and octahedral voids, with a relatively low energy barrier of 0.62 eV. The Li diffusion barrier can be further reduced by applying hydrostatic pressure to the fullerene structure, which essentially represents a model for polymerized fullerene. The lowering of the barrier continues till a volume strain of 17.7% is reached corresponding to a pressure value of 1.19 GPa and is caused by the combined effect of rapid charge transfer from the Li to the fullerene and the modification of the profile of the local potential, which becomes more attractive for the Li with the increasing pressure. Experimentally, this

amount of pressure can easily be applied. The lowering of the barrier causes a two orders of magnitude increase in Li diffusivity. Therefore, the pressurized fullerene having high diffusivity of Li, can be used as an artificial solid electrolyte interface for an anode to achieve a faster rechargeable battery. Beyond the 17.7% of volume strain, the C–C bond formation between the atoms of adjacent fullerenes leads to an increase in the energy barrier for the Li diffusion. This sets up a limit to the applied strain in obtaining the high diffusion rates in the polymerized fullerene based artificial SEI.

Acknowledgements

D.D. and A.K.S. thankfully acknowledge the financial support from Korea Institute of Science and Technology (Grant No. 2E23920), S.S. Han and K.-R.L. were supported by the Industrial Strategic Technology Development Program (Grant No. 10041589) funded by the Ministry of Knowledge Economy (MKE, Korea). We thankfully acknowledge the Materials Research Centre and Supercomputer Education and Research Centre, Indian Institute of Science for computing facilities.

References

1 K. Kang, Y. S. Meng, J. Bréger, C. P. Grey and G. Ceder, *Science*, 2006, **311**, 977–980.
2 B. Kang and G. Ceder, *Nature*, 2009, **458**, 190–193.
3 J. B. Goodenough and K.-S. Park, *J. Am. Chem. Soc.*, 2013, **135**, 1167–1176.
4 R. V. Noorden, *Nature*, 2014, **507**, 26–28.
5 J. Goodenough and Y. Kim, *J. Power Sources*, 2011, **196**, 6688–6694.
6 M.-K. Song, E. J. Cairns and Y. Zhang, *Nanoscale*, 2013, **5**, 2186–2204.
7 M. S. Whittingham, *MRS Bull.*, 2008, **33**, 411–419.
8 J.-M. Tarascon and M. Armand, *Nature*, 2001, **414**, 359–367.
9 V. Etacheri, R. Marom, R. Elazari, G. Salitra and D. Aurbach, *Energy Environ. Sci.*, 2011, **4**, 3243–3262.
10 Y. Nishi, *J. Power Sources*, 2001, **100**, 101–106.
11 J. P. Maranchi, A. F. Hepp and P. N. Kumta, *Electrochem. Solid-State Lett.*, 2003, **6**, A198–A201.
12 T. D. Hatchard and J. R. Dahn, *J. Electrochem. Soc.*, 2004, **151**, A838–A842.
13 M. T. McDowell, S. W. Lee, I. Ryu, H. Wu, W. D. Nix, J. W. Choi and Y. Cui, *Nano Lett.*, 2011, **11**, 4018–4025.
14 M. T. McDowell, I. Ryu, S. W. Lee, C. Wang, W. D. Nix and Y. Cui, *Adv. Mater.*, 2012, **24**, 6034–6041.
15 C. K. Chan, H. Peng, G. Liu, K. McIlwrath, X. F. Zhang, R. A. Huggins and Y. Cui, *Nat. Nanotechnol.*, 2008, **3**, 31–35.
16 B. Wang, X. Li, X. Zhang, B. Luo, M. Jin, M. Liang, S. A. Dayeh, S. T. Picraux and L. Zhi, *ACS Nano*, 2013, **7**, 1437–1445.
17 A. A. Arie, J. O. Song and J. K. Lee, *Mater. Chem. Phys.*, 2009, **113**, 249–254.
18 E. Lee and K. A. Persson, *Nano Lett.*, 2012, **12**, 4624–4628.
19 D. Das, S. Kim, K.-R. Lee and A. K. Singh, *Phys. Chem. Chem. Phys.*, 2013, **15**, 15128–15134.
20 E. Pollak, B. Geng, K.-J. Jeon, I. T. Lucas, T. J. Richardson, F. Wang and R. Kostecki, *Nano Lett.*, 2010, **10**, 3386–3388.
21 H. W. Kroto, J. R. Heath, S. C. O'Brien, R. F. Curl and R. E. Smalley, *Nature*, 1985, **318**, 162–163.
22 H. Tachikawa, *J. Phys. Chem. C*, 2011, **115**, 20406–20411.
23 Y. Wang, D. Tománek and G. F. Bertsch, *Phys. Rev. B: Condens. Matter Mater. Phys.*, 1991, **44**, 6562–6565.
24 A. A. Arie and J. K. Lee, *Phys. Scr.*, 2010, **2010**, 014013.
25 A. Arie, W. Chang and J. Lee, *J. Solid State Electrochem.*, 2010, **14**, 51–56.
26 A. Arie and J. Lee, *J. Ceram. Process. Res.*, 2009, **10**, 614–617.
27 C. S. Sundar, P. C. Sahu, V. S. Sastry, G. V. N. Rao, V. Sridharan, M. Premila, A. Bharathi, Y. Hariharan, T. S. Radhakrishnan, D. V. S. Muthu and A. K. Sood, *Phys. Rev. B: Condens. Matter Mater. Phys.*, 1996, **53**, 8180–8183.
28 H. Yamawaki, M. Yoshida, Y. Kakudate, S. Usuba, H. Yokoi, S. Fujiwara, K. Aoki, R. Ruoff, R. Malhotra and D. Lorents, *J. Phys. Chem.*, 1993, **97**, 11161–11163.
29 G. Kresse and J. Hafner, *Phys. Rev. B: Condens. Matter Mater. Phys.*, 1993, **47**, 558–561.
30 G. Kresse and D. Joubert, *Phys. Rev. B: Condens. Matter Mater. Phys.*, 1999, **59**, 1758–1775.
31 P. E. Blöchl, *Phys. Rev. B: Condens. Matter Mater. Phys.*, 1994, **50**, 17953–17979.
32 J. P. Perdew, K. Burke and M. Ernzerhof, *Phys. Rev. Lett.*, 1996, **77**, 3865–3868.
33 G. Kresse and J. Furthmüller, *Comput. Mater. Sci.*, 1996, **6**, 15–50.
34 S. Grimme, *J. Comput. Chem.*, 2006, **27**, 1787–1799.
35 R. L. Whetten, *The MRS late News Session-Buckeyballs: New Materials Made from Carbon Soot, Videotape*, Materials Research Society, Pittsburgh, 1990.
36 S. Saito and A. Oshiyama, *Phys. Rev. Lett.*, 1991, **66**, 2637–2640.
37 G. Henkelman, B. P. Uberuaga and H. Jónsson, *J. Chem. Phys.*, 2000, **113**, 9901.
38 K. Persson, V. A. Sethuraman, L. J. Hardwick, Y. Hinuma, Y. S. Meng, A. van der Ven, V. Srinivasan, R. Kostecki and G. Ceder, *J. Phys. Chem. Lett.*, 2010, **1**, 1176–1180.
39 K. Toyoura, Y. Koyama, A. Kuwabara, F. Oba and I. Tanaka, *Phys. Rev. B: Condens. Matter Mater. Phys.*, 2008, **78**, 214303.
40 S. J. Duclos, K. Brister, R. C. Haddon, A. R. Kortan and F. A. Thiel, *Nature*, 1991, **351**, 380–382.
41 Y. Iwasa, T. Arima, R. M. Fleming, T. Siegrist, O. Zhou, R. C. Haddon, L. J. Rothberg, K. B. Lyons, H. L. Carter, A. F. Hebard, R. Tycko, G. Dabbagh, J. J. Krajewski, G. A. Thomas and T. Yagi, *Science*, 1994, **264**, 1570–1572.
42 B.-L. Gu, Y. Maruyama, J.-Z. Yu, K. Ohno and Y. Kawazoe, *Phys. Rev. B: Condens. Matter Mater. Phys.*, 1994, **49**, 16202–16206.
43 Y.-N. Xu, M.-Z. Huang and W. Y. Ching, *Phys. Rev. B: Condens. Matter Mater. Phys.*, 1992, **46**, 4241–4245.
44 H. Hirai and K.-i. Kondo, *Phys. Rev. B: Condens. Matter Mater. Phys.*, 1995, **51**, 15555–15558.